

MECHANICAL CHARACTERIZATION OF MICROLAMINAR STRUCTURES EXTRACTED FROM CELLULOSIC MATERIALS USING NANOINDENTATION TECHNIQUE

EMILIO RAYÓN, JUAN LÓPEZ* and MARINA P. ARRIETA**

*Technological Institute of Materials, Universitat Politècnica de València, Camí de Vera s/n. E46022,
Valencia, Spain*

**Technological Institute of Materials, Universitat Politècnica de València,
03801 Alcoy-Alicante, Spain*

***Analytical Chemistry, Nutrition and Food Sciences Department, University of Alicante,
P.O. Box 99, E-03080 Alicante, Spain*

Received November 15, 2012

Nanohardness (H) and elastic modulus (E) properties of several biomass by-products (fruit shells) have been characterized by nanoindentation technique. Two procedures were followed: (i) 3D topographic images for the microstructure characterization and (ii) 2D mechanical mapping for density and mechanical distribution features analysis.

Results revealed the typical cellulosic cell wall structures, indicating that the reduced modulus values (E_r) for the cellulosic cells and the amorphous matrix phases were of 6.2 GPa and 4 GPa, respectively, for the apricot shell. The single phases of the rest of structures were tested, showing differences in modulus due to the content of cellulose in the hierarchical structure, and various H and E_r features for each specimen and microstructure analyzed.

Keywords: nanoindentation, mechanical properties, cellulosic biomaterials

INTRODUCTION

Nowadays, the agricultural industries generate tons of waste that can be recovered, such as fruit shells. A possible use of this 'environmentally friendly material' is to burn it for bioenergy and biochemicals production.¹ Nevertheless, their biodegradability properties could help to reduce the environmental degradation by means of manufacturing biodegradable composites.²⁻⁶ Wood possesses key advantages, compared to other biodegradable materials, in terms of wide availability in a range of densities, renewability, and low cost.⁷ The most important attribute of wood is its excellent mechanical performance at comparably low weight, as well as the use of wood as structural material.⁸

The structure of wood extracted from a plant or tree is characterised by long semi-crystalline cellulosic microfibrils of thick-walled hollow

cells, which form channels for water transport.⁹⁻¹¹ Although the chemical composition is identical with that of wood, the structure of fruit shell is expected to be different because water transport is not required for long distances. Recently, Kaupp *et al.*¹² characterized several nutshells, showing shorter fibrous elliptical or spherical cells in various arrangements. The morphological differences found in these cellulosic materials confer to seed shells the required mechanical properties to protect the seed from falls, knocks, bites, etc.

The mechanical and microstructure properties of cellulose structures have been well studied for several decades at the macroscale. Nowadays, the scientific community of biomaterials is focusing their attention on the mechanical properties at the micro¹³ and nanoscale.¹⁴⁻¹⁷ The mechanical

properties for a small volume of material are studied by means of Instrumented Indentation Techniques (IIT), such as Atomic Force Microscopes (AFM) and nanoindentation machines.

A nanoindenter is an apparatus that serves to determine the hardness (H) and elastic modulus (E) in nanometric volumes of material.¹⁸⁻²⁰ The very low loads used in these measurements permit us to analyze the mechanical properties of each single constituent in a hierarchical structure at the nanoscale.¹⁹⁻²² The H and E from IIT data are calculated without direct measurement of the indented imprint.²³⁻²⁶ Thus, the H and E features are calculated using the load (P) and penetration depth (h) data curves.

The aim of this paper has been to evaluate two fast procedures to study the nano- and micromechanical properties of biomass by-product materials (fruit shells), using a nanoindenter machine. The optimized procedure was successfully applied in several fruit shells studies: nuts, hazelnuts, walnuts and peaches. By means of several indentation tests performed at 1000 nm depth, the H and elastic modulus (E_r) profiles were acquired for each constituent of the structure. Two strategies were probed: a 2D mechanical map and a 3D topographic image acquired by the same tip used for indent.

EXPERIMENTAL

Several cellulose microstructures of *Juglans regia* (walnut), *Corylus avellana* (hazelnut), *Prunus armeniaca* (apricot), *Prunus persica* (peach) and *Prunus dulcis* (almond) were analyzed. Stones were cut along their cross-section under dry conditions using a diamond knife and abrasive papers. Samples were kept in a box for one year at constant 30% humidity. In order to perform the experiment under the same humidity conditions, silica gel was introduced in the cabinet of the nanoindenter for a week, ensuring the same humidity level by hygrometer.

The mechanical properties and 3D images were acquired by a nanoindenter G-200 (Agilent Technologies, USA) with a previously calibrated Berkovich diamond tip. The indenter shape was carefully calibrated using a fused silica as a reference material with a well-known elastic modulus of 72 GPa, ensuring a radius of the tip below 20 nm. Experiments were carried out by Continuous Stiffness Measurement (CSM)²⁷, with 70 Hz of harmonic oscillation frequency and 2 nm of harmonic amplitude. Indentations were programmed at a constant 1000 nm depth. As the materials essayed have no isotropic behavior, the choice of Poisson's ratio used in Young's Modulus calculation is not ascertainable at all. Young's

Modulus calculated by nanoindentation has nothing in common with the modulus from a tensile test and the elastic behavior in wood based materials, because the evaluation of indents is carried out using isotropic indentation theory.^{23,24} Consequently, the term 'Young's Modulus' as frequently used to describe the nanoindentation results would be incorrect here. This is the reason why for similar materials (like wood) typically just the reduced modulus, E_r (indentation modulus) is compared as relative value.^{28,29} Recently, some approaches have been shown in order to monitor the dependence of the orthotropic properties of the E_r and vice versa.³⁰ In this work, the elastic modulus is calculated as E_r .

The microstructures were characterized by 3D images using the Nanovision^(R) technology, which uses the same indenter head to scan topographically the surface of samples in the contact mode. Images were acquired before and after the indentation tests with a contact force of 3 μ N. For the mechanical 2D mapping representations, a grid of 450 indentations with a distance of 40 μ m among them was performed, it achieving a total area of 400 μ m x 1800 μ m.

RESULTS AND DISCUSSION

Nanoindentation results using 3D images

Figure 1 shows the 3D topographic image acquired on the cross-section of the apricot shell, distinguishing several Berkovich imprints performed at 1000 nm depth (marked by arrows). This image firstly corroborates that each phase of the hierarchical structure can be distinguished by hardness differences. Furthermore, these images have enough resolution to locate and resolve the subsequent locations to perform the subsequent indentations. Although it seems that the apparent roughness could be affected in a great manner in the acquired H results, flat surfaces were found and a narrow scattering for H values at small depths were recorded, as shown by the subsequent results. Moreover, this image corroborates that the apricot shell is built up by the typical vascular tissue formed by cellulose cells, whose diameters are from 20 μ m to 40 μ m. The cellulose cells are found with other neighbour cells and with a zone that did not present the typical cell structure (less crystalline cellulose), which was assumed to be the matrix. This matrix or the space filled between the wood cells is probably formed by hemicelluloses and lignin. The P - h curve acquired for each indentation test is shown in Figure 2. Several relaxation pop-in events were recorded at 3 μ N and 4 μ N. These events differ from those occurring for metals or ceramic materials,³¹ whose deformations are based on dislocation movements. The characteristic pop-in event for

these materials is a flat curve maintained along several nanometres. Nevertheless, the recorded pop-in events on this cellulosic material are not flat, showing a sloped curve instead. We assume that these events could be due to the roughness of surfaces and to the elastic-plastic transition mechanism. However, we think that they are due to the characteristic deformation mechanism of these kinds of materials. The displacements occurring in the cell wall interfaces under mechanical stress are governed by molecular bonds, which transmit shear stresses between the cellulose fibrils. Keckes *et al.*³² demonstrated that when a certain shear stress is exceeded, the bonds of the cell wall interfaces break and a viscous flowing occurs as regards the matrix. As soon as the stress is released, the unspecific bonds re-form immediately in the new position (like a stick-slip connection that has been opened and closed). An instrumented indentation equipment should be sensitive enough to provide information about these events explaining the recorded $P-h$ curve.

Figure 3 shows the resulted mean H values on the cell and matrix microstructures of the apricot shell, while the indentation imprints were monitored by 3D images. These curves revealed a gradual increase of H , from 100 MPa at 100 nm, up to 200 MPa at 1000 nm.

This behaviour contradicts the expected increase of hardness with decreasing the indention load or indentation depth,^{28,33} also known as the

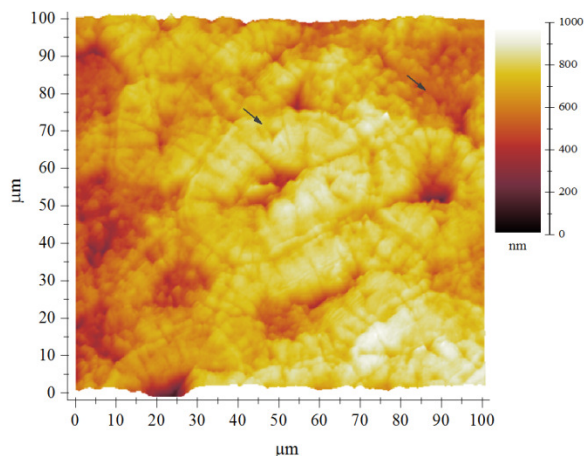


Figure 1: 3D image of the microstructure acquired on apricot shell. The arrows indicate several imprints on cells and matrix generated by nanoindentation at 1000 nm depth

Indentation Size Effect, ISE. Figure 4 displays the same H and E_r tendency. We think that this inverse behaviour is due to the manner stresses are distributed beyond the indenter and to the great changes within the interaction volume, which will dominate the deformation response. Furthermore, the cellulose-fibril angle beyond a pyramidal indenter is expected to be different depending of the depth reached. This is, the cells by themselves do not generate shear stresses, but the indenter geometry may induce both normal and shear stresses,³⁰ increasing the stiffness response at higher indented volumes (higher shear component). This effect was observed previously,¹³ but further efforts should be focused on this aspect in order to clarify this mechanism. Figure 5 shows that the E_r curves for cellulosic cells were kept constant in depth, at an average value of 6.2 GPa. Furthermore, two trends were observed in the E_r curves below the 500 nm depth. This is, while the E_r value on the cell wall reached 6.2 GPa, the test performed on the matrix resulted in 4 GPa. This difference is expected since the cells are composed of 100% cellulose, while the matrix is probably a mixture of hemicelluloses and lignin. Thus, there is a greater amount of molecular mobility in the matrix than in the cell wall.³⁴ In fact, the differences between a softwood and hardwood are due to the content of these components.

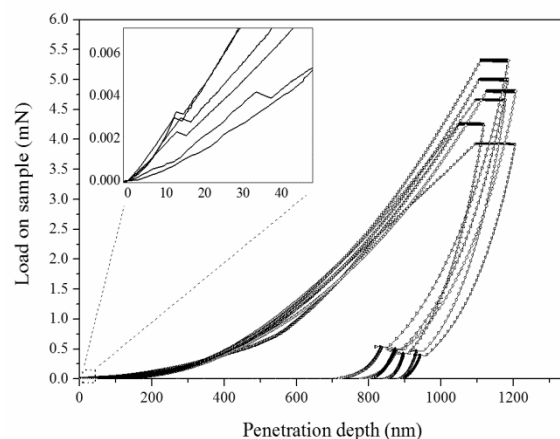


Figure 2: $P-h$ nanoindentation curves recorded the apricot shell indented on cross-section. The in-set figure is a detail of the pop-in events recorded

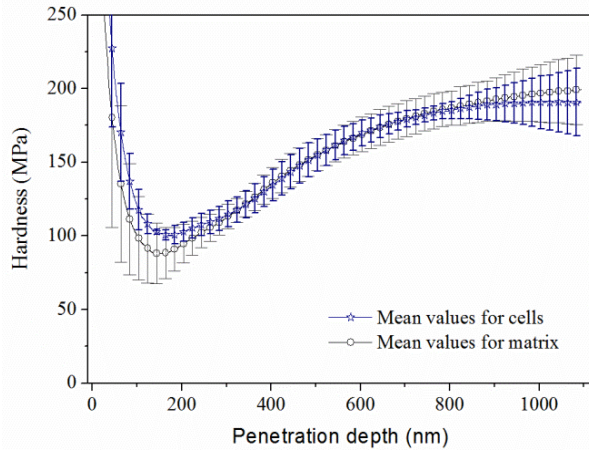


Figure 3: Hardness mean values for cell and matrix microstructures of the apricot shell

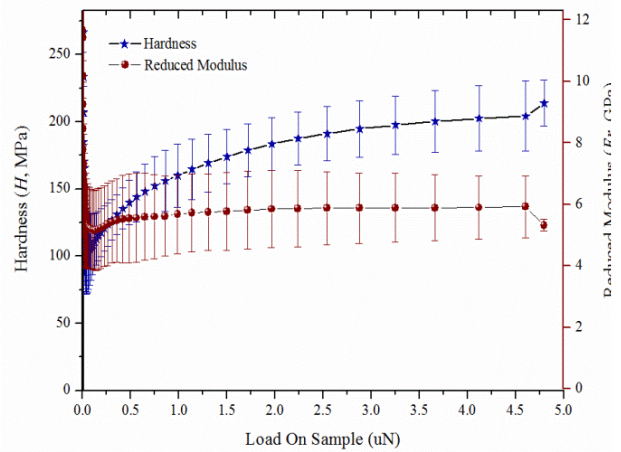


Figure 4: Hardness and reduced modulus versus indented load

Exceeding the 500 nm depth, all curves tended to converge indicating that an average value of all phases was obtained. However, these trends were less clear in the H profiles, probably due to the manner the shear stresses were distributed beyond the tip.

Similar results were acquired for the rest of the analysed species. Figure 6 summarizes the most representative 3D microstructures for the rest of fruit shells tested. Differences in cell morphology and relative density (elliptical or spherical cells in various arrangements) can be distinguished for each specimen analyzed.

Figure 7 summarizes comparative H and E_r values, averaging results in the 50-100 nm range of depth. Note that the H value highly depends on the selected depth. This range has been chosen considering the minimum possible penetration depth to achieve differences between phases, while it assures a measure without the expected error due to the tip roundness. The great differences found in the H and E_r values for the essayed species could be explained by the difference in density and microfibril angles for each species.

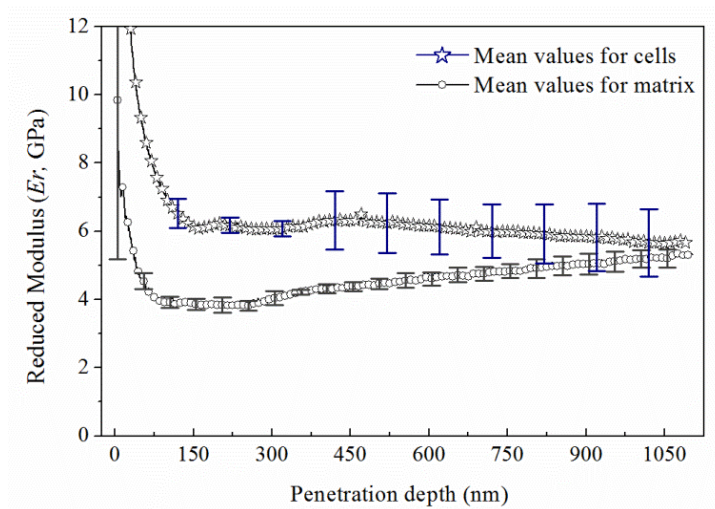


Figure 5: Modulus mean values for cell and matrix microstructures of the apricot shell

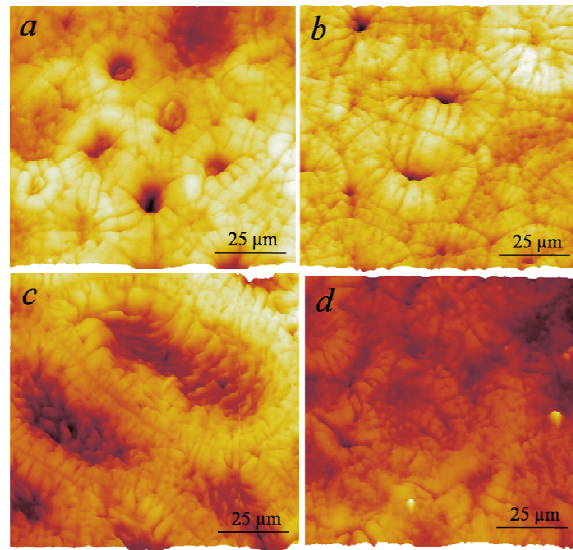


Figure 6: Microstructure 3D images of the surfaces of hazelnut (a), almond (b), peach (c) and walnut (d) stones

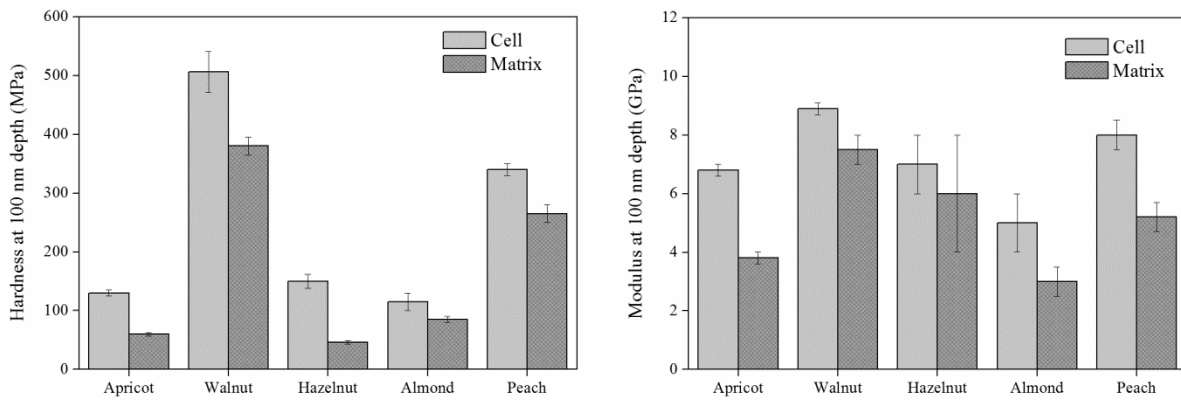


Figure 7: Summary of the resulted hardness and modulus for the specimens under study

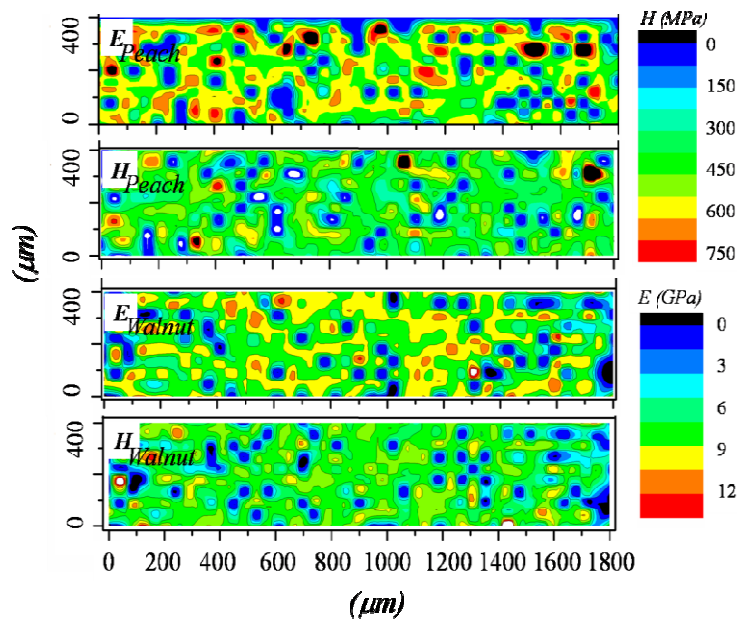


Figure 8: Distribution maps of hardness and modulus features acquired on the cross-sectional view for peach and walnut seeds by nanoindentation

2D distribution mappings

The second strategy followed was to plot 2D mechanical maps.^{20,35} The aim of this strategy was to monitor the distribution of the H and E_r along the entire thickness of the seed shell. As a square form will lead to a great matrix, a grid of 450 indents distributed on an area of 1800 μm x 400 μm was experimented and the acquired results were then represented by a colored scale. The indented area covered the entire sheet width. Figure 8 shows the H and E_r results for a grid of 450 indentations performed on the peach and walnut stone shells. The outer bark of the shell is situated on the right of the map, while the inner bark is on the left. These results are in agreement with those obtained by 3D imaging with the advantage that the population of test is higher in a minor operator's consumed time. This procedure is especially interesting when a great number of population tests or specimens are studied. Furthermore, it permits to visualize the distribution of the mechanical properties in the width of the shell and gives an idea of the density distribution in the material. Figure 8 also demonstrates that the values of hardness were homogeneously distributed (the green colors predominate), while the measured modulus was higher for cells.

Further investigations should be focused on the microstructure features, the hemicelluloses and lignin content, local density and MFA of these materials in order to clarify the mechanical differences found. However, the information extracted from these studies could help understand and develop new models on the mechanical responses of other natural materials. These studies will be carried out in a forthcoming work.

CONCLUSION

The nanoindentation technique has proven useful to study the hardness and elastic modulus of several hierarchical structures extracted from agriculture industry. The single phases of the hierarchical structure were tested showing differences in their elastic modulus properties. Several 3D microstructures were revealed for each fruit stone. These morphologies could be the cause of the mechanical differences found for each specimen. The 2D mechanical maps showed the same results achieving micrometer areas. This procedure is useful when local densities must be compared, e.g. the kernel and outer bark or inner

bark of the seed. Nevertheless, we avoided an in-depth compositional, density and microfibril angle study. This analysis showed that nanoindentation could be a useful technique to differentiate biocellulosic structures, according to their nanoscale mechanical properties.

ACKNOWLEDGEMENTS: This work has been supported by the Spanish Ministry of Science and Innovation (MAT2011-28468-C02-02) and the Autonomous Government of Valencia (Spain) through the research program Gerónimo Forteza (62/2010, 9 de Junio DOCV n° 6291) and Santiago Grisolia fellowship (M. P. Arrieta GRISOLIA/2011/007).

REFERENCES

- ¹ G. Chinga-Carrasco, *Nanoscale Res. Lett.*, **6**, 417 (2011).
- ² A. K. Bledzki, J. Gassan, *Progr. Polym. Sci.*, **24**, 221 (1999).
- ³ A. S. Galperin, G. G. Kuleshov, V. I. Tarashkevich, G. M. Shutov, *Holzforschung*, **49**, 45 (1995).
- ⁴ J. E. Crespo, L. Sanchez, F. Parres, J. Lopez, *Polym. Composite.*, **28**, 71 (2007).
- ⁵ J. E. Crespo, R. Balart, L. Sanchez, J. Lopez, *Int. J. Adhes.*, **27**, 422 (2007).
- ⁶ J. A. Meyer, *Wood Sci.*, **14**, 49 (1981).
- ⁷ M. P. Ansell, *J. Mater. Sci.*, **47**, 583 (2012).
- ⁸ J. Konnerth, N. Gierlinger, J. Keckes, W. Gindl, *J. Mater. Sci.*, **44**, 4399 (2009).
- ⁹ B. A. Meylan, B. G. Butterfield, *Wood Sci. Technol.*, **12**, 219 (1978).
- ¹⁰ F. V. Vincent Julian, *Curr. Opin. Solid St. M.*, **3**, 228 (1998).
- ¹¹ S. Y. Zhang, *Wood Sci. Technol.*, **31**, 181 (1997).
- ¹² G. Kaupp, M. R. Naimi-Jamal, *J. Mater. Chem.*, **21**, 8389 (2011).
- ¹³ J. E. Jakes, D. S. Stone, C. R. Frihart, in *Procs. 30th Annual Meeting of the Adhesion Society Inc.*, February 18-21, 2007, Tampa Bay, FL. (2007), pp. 15-17.
- ¹⁴ W. Gindl, H. S. Gupta, *Compos., A-App. Sci.*, **33**, 1141 (2002).
- ¹⁵ X. Zhang, Q. Zhao, S. Wang, R. Trejo, E. Lara-Curzio *et al.*, *Compos. Part a-App. Sci.*, **41**, 632 (2010).
- ¹⁶ R. Wimmer, B. N. Lucas, T. Y. Tsui, W. C. Oliver, *Wood Sci. Technol.*, **31**, 131 (1997).
- ¹⁷ L. Zou, H. Jin, W.-Y. Lu, X. Li, *Mater. Sci. Eng. C-Biomim.*, **29**, 1375 (2009).
- ¹⁸ E. Rayon, V. Bonache, M. D. Salvador, J. J. Roa, E. Sanchez, *Surf. Coat. Tech.*, **205**, 4192 (2011).
- ¹⁹ S. Pathak, J. Michler, K. Wasmer, S. R. Kalidindi, *J. Mater. Sci.*, **47**, 815 (2012).
- ²⁰ E. Rayón, V. Bonache, M. D. Salvador, E. Bannier, E. Sánchez, *et al.*, *Surf. Coat. Tech.*, **206**, 2655 (2011).

- ²¹ J. E. Jakes, D. S. Stone, *Philos. Mag.*, **91**, 1387 (2011).
- ²² T. Ohmura, K. Tsuzaki, *J. Mater. Sci.*, **42**, 1728 (2007).
- ²³ W. C. Oliver, G. M. Pharr, *J. Mater. Res.*, **7**, 1564 (1992).
- ²⁴ W. C. Oliver, G. M. Pharr, *J. Mater. Res.*, **19**, 3 (2004).
- ²⁵ R.-B. Adusumalli, W. M. Mook, R. Passas, P. Schwaller, J. Michler, *J. Mater. Sci.*, **45**, 2558 (2010).
- ²⁶ Y. T. Cheng, C. M. Cheng, *Mat. Sci. Eng. R.*, **44**, 91 (2004).
- ²⁷ X. D. Li, B. Bhushan, *Mat. Charac.*, **48**, 11 (2002).
- ²⁸ W. T. Y. Tze, S. Wang, T. G. Rials, G. M. Pharr, S. S. Kelley, *Compos., A-App. Sci.*, **38**, 945 (2007).
- ²⁹ W. Gindl, T. Schoberl, *Compos., A-App. Sci.*, **35**, 1345 (2004).
- ³⁰ A. Jaeger, T. Bader, K. Hofstetter, J. Eberhardsteiner, *Compos., A-App. Sci.*, **42**, 677 (2011).
- ³¹ J. J. Roa, E. Rayon, M. Morales, M. Segarra, *Recent Patents on Nanotechnology*, **6**, 142 (2012).
- ³² J. Keckes, I. Burgert, K. Fruhmann, M. Muller, K. Kolln, *et al.*, *Nat. Mater.*, **2**, 810 (2003).
- ³³ E. Manika, J. Maniks, *Acta Mater.*, **54**, 2049 (2006).
- ³⁴ C. A. S. Hill, J. Ramsay, B. Keating, K. Laine, L. Rautkari, *et al.*, *J. Mater. Sci.*, **47**, 3191 (2012).
- ³⁵ V. Canseco, J. J. Roa, E. Rayon, A. I. Fernandez, E. Palomo, *Ceram. Int.*, **38**, 401 (2012).